IET Radar, Sonar & Navigation

Special Issue Call for Papers

Be Seen. Be Cited.
Submit your work to a new IET special issue

Connect with researchers and experts in your field and share knowledge.

Be part of the latest research trends, faster.

Read more

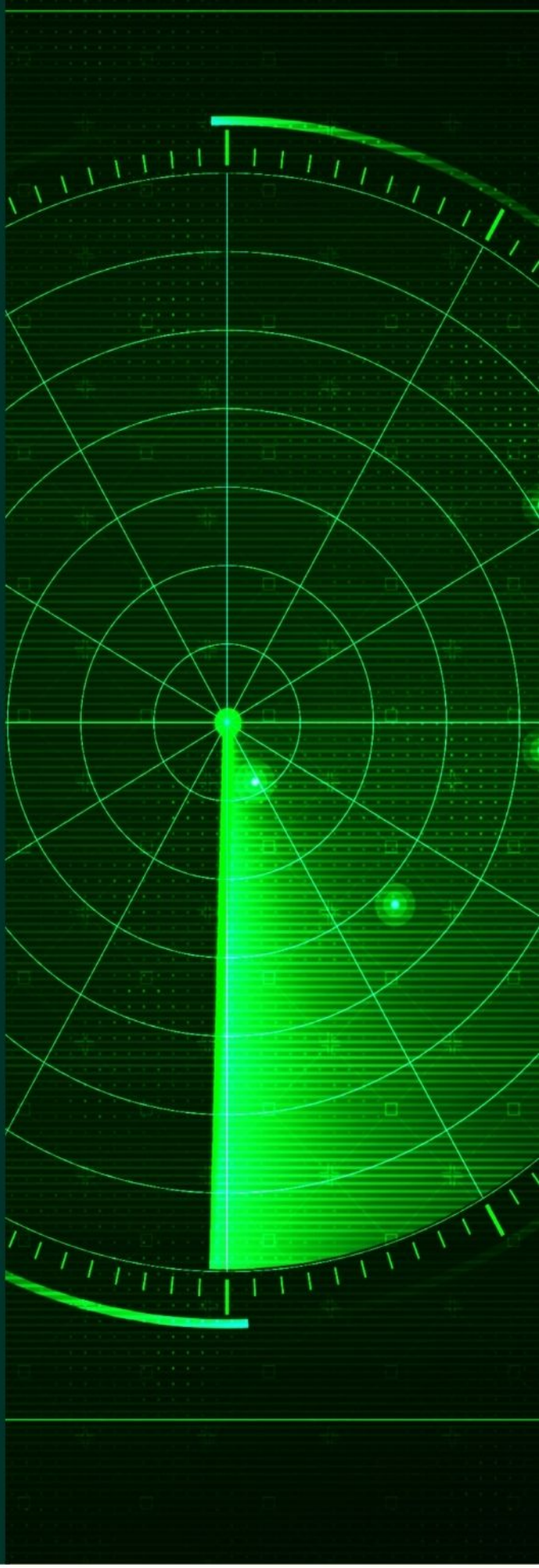

The Institution of Engineering and Technology

IET Radar, Sonar & Navigation

Research Article

IET Journals
The Institution of Engineering and Technology

Integrated waveform for continuous active sonar detection and communication

ISSN 1751-8784
Received on 28th February 2020
Revised 25th April 2020
Accepted on 6th May 2020
E-First on 23rd July 2020
doi: 10.1049/iet-rsn.2020.0099
www.ietdl.org

Jingwei Yin[1,2,3], *Wei Men*[1,2,3], *Xiao Han*[1,2,3] ✉, *Longxiang Guo*[1,2,3]

[1]*Acoustic Science and Technology Laboratory, Harbin Engineering University, Harbin 150001, People's Republic of China*
[2]*Key Laboratory of Marine Information Acquisition and Security (Harbin Engineering University), Ministry of Industry and Information Technology, Harbin 150001, People's Republic of China*
[3]*College of Underwater Acoustic Engineering, Harbin Engineering University, Harbin 150001, People's Republic of China*
✉ *E-mail: hanxiao1322@hrbeu.edu.cn*

Abstract: A novel integrated waveform (IW) for continuous active sonar detection and communications is proposed in this study based on a generalised sinusoidal frequency-modulated signal. This study first introduces the mixed modulation of the IW and a model for the transmitting signal, and then it analyses the time and frequency resolution and anti-reverberation capability of the proposed IW. The performance of two underwater acoustic (UWA) communication receivers based on the proposed IW are compared and analysed under Gaussian noise and multipath conditions. A UWA communication experiment was carried out in Songhua Lake in December 2019. According to the numerical simulation and experimental results, it was concluded that the IW proposed in this study can meet the requirements of active sonar detection and UWA communications with satisfactory performance.

1 Introduction

The integration of detection and communication (IDC) technology was first studied for radar. As early as the 1960s, Mealey [1] proposed using radar for communications, and realised a one-way communication system by modulating communication data with radar pulses. In the 1970s, the United States Navy placed one radar in a laboratory in the Western Chesapeake Bay and another on Tilghman Island. This experiment proved to some extent the feasibility of integrated radar and communication [2]. Compared with the integration of radar and communication on land, due to the complexity of underwater acoustic (UWA) channels, underwater IDC is still in its infancy and little work has been reported. Lu from Northwest Polytechnical University undertook a brief analysis of the detection performance of three conventional single-carrier UWA modulation signals [minimum-shift keying, two-frequency frequency-shift keying, and binary phase-shift keying (BPSK)] by comparing their ambiguity function (AF) and Q function [3].

There are three types of IDC systems: time-sharing systems, beam-splitting systems, and simultaneous systems. Compared with the other two systems, a simultaneous system with the same beam has the highest integration, but is the most difficult to realise. The design methods of simultaneous system's integrated waveform (IW) can be divided into two categories based on communication signals and detection signals according to the primary and secondary division of detection and communication functions.

At present, research into IWs based on communication signals in radar is mainly based on orthogonal frequency division multiplexing (OFDM) signals. The earliest application of OFDM signals for radar was by Jankiraman *et al.* [4, 5], who developed PANDORA. This is a multicarrier radar system using microwave power synthesis. Levanon's research into OFDM-coded radar used a multicarrier phase-coded radar signal. By adding P4 Huffman codes and other codes into the OFDM signal, the autocorrelation of the signal and the target resolution were improved [6, 7]. IWs can also be based on spread spectrum signals. Xu *et al.* [8] proposed an IW synthesis method based on the orthogonal sequence of a spread spectrum. The receiver was separated so that signals were processed by decoding a spread spectrum to obtain the communication information. Jamil *et al.* [9] proposed an integrated radar and communication system that utilises weighted pulse trains with the elements of Oppermann sequences serving as complex weights.

Research into IWs based on detection signals is mainly based on linear frequency modulation (LFM) signals. Xie *et al.* [10] and Chen *et al.* [11] encoded the communication information by modulating the LFM signal. Roberton and Brown [12] used up-chirp LFM and down-chirp LFM to realise communication and radar functions, respectively. The IWs obtained by these methods can realise the functions of radar detection and communication at the same time, but the inevitable problem is that the communication rate is low, making it difficult to meet most actual communication requirements. Zhang *et al.* [13–15] combined BPSK with an LFM signal to integrate radar and communication signals. Further, the communication information was hidden in the integrated signal using reducing phase-shift keying (RPSK) and variable symbol duration.

Active sonar detection and UWA communication are indispensable underwater information technologies for surface and underwater combat platforms, so realising underwater IDC has a great significance. However, due to the complexity of the UWA channel, such as the serious multipath interference, the Doppler effect, and the channel time variability, many methods for integrating radar and communications cannot be applied underwater. The target detection capability is the key factor in the success or failure of an underwater platform used for electronic countermeasures. So the design of IWs based on the detection signals is the main development direction. The aim is to achieve efficient embedding and demodulation of communication information while maintaining detection performance.

Continuous active sonar (CAS) is a bi-static system that transmits high duty cycle waveforms. It has a higher target revisit rate and better tracking recognition than conventional pulse active sonar [16–20]. Moreover, CAS-IDC systems have a good communication rate. Generalised sinusoidal frequency-modulated (GSFM) signals are nearly orthogonal to each other, even when occupying the same band of frequencies, and they have an approximate thumbtack AF. Furthermore, GSFM can achieve the minimum estimation variance for the time delay and Doppler shift, and have an optimal resolution of closely spaced targets in range and Doppler shift [20, 21]. Due to the low mutual interference and

the high range and velocity resolution, GSFM pulses have been applied in CAS systems [20].

In this paper, an IW for CAS detection and communication is proposed based on the GSFM signal. Digital information is embedded into the GSFM waveform, and we call this IW the GSFM-com signal. In terms of target detection, an analysis of the AF and Q function has shown that the GSFM-com signal has a high range and velocity resolution and strong anti-reverberation ability. The communication rate of a GSFM-com signal is much higher than that of the IWs [10–12] based on the detection signal in the radar. In the IDC receiver, a matched filter receiver (MFR) is used to process the RPSK-modulated LFM signal [15]. However, the receiver is very sensitive to any multipath interference in the UWA channel, which seriously affects the decoding performance of the communication system. A decision feedback equaliser [22, 23] has strong tracking performance for the channel structure because updating the coefficients eliminates the inter-code interference generated by the multipath channel. So, in this paper, a multichannel decision feedback equaliser receiver (DFER) is used to process GSFM-com signals received by each array element at the communication receiving end. A field communication experiment on the GSFM-com signal was conducted in Songhua Lake, Jilin Province, China, and the results showed that both single-channel DFER and multichannel DFER can be decoded without error.

The remainder of this paper is organised as follows. Section 2 briefly describes the GSFM signal, the GSFM-com signal, and the transmission signal model for CAS-IDC. Section 3 analyses the detection performance of GSFM-com, including range and velocity resolution and reverberation suppression. Section 4 describes two receiver algorithms for the receiving end of the communication and compares their performance using a numerical simulation. Section 5 presents the experimental results. Finally, a summary and concluding remarks are provided in Section 6.

2 IW based on a GSFM signal

2.1 GSFM waveform

The GSFM signal proposed by Hague and Buck [20, 21] modifies a sinusoidal frequency-modulated waveform using an instantaneous frequency (IF) function that resembles a frequency-modulated chirp waveform. Thus, GSFM has a frequency modulation waveform expressed as follows:

$$g(t) = \frac{\text{rect}(t)}{\sqrt{T}} e^{j\phi_{\text{GSFM}}(t)} e^{j2\pi f_c t}, \tag{1}$$

where rect(t) is the rectangular function, T is the signal duration time, $\phi_{\text{GSFM}}(t)$ is the phase modulation function, and f_c is the centre frequency. The phase function and IF function for GSFM are

$$\phi_{\text{GSFM}}(t) = \frac{\beta}{t^{(\rho-1)}} \sin\left(\frac{2\pi\alpha t^{\rho}}{\rho}\right) \tag{2}$$

and

$$f_{\text{GSFM}}(t) = \beta\alpha\left[\cos\left(\frac{2\pi\alpha t^{\rho}}{\rho}\right) - \left(\frac{\rho-1}{\rho}\right)\text{sinc}\left(\frac{2\pi\alpha t^{\rho}}{\rho}\right)\right], \tag{3}$$

where the modulation index $\beta = B/2\alpha$. B is the bandwidth of the signal, and α is a frequency modulation term with units $s^{-\rho}$. The number of cycles in the IF of the GSFM $C = \alpha T^{\rho}/\rho$, where $\rho \geq 1$ is a dimensionless parameter. When $\rho = 1$, the GSFM signal degenerates into a sinusoidal frequency-modulated signal.

Conventional active sonar waveforms use an LFM signal to partition the frequency band to produce pulses that are orthogonal to each other, which results in very low-frequency band utilisation. This method is limited by the underwater frequency band. However, by changing the parameters α and ρ, GSFM signals can easily produce many waveforms that are nearly orthogonal to each other and occupy the same frequency band. Fig. 1 shows the cross-correlation of two GSFM pulses with different parameters and same frequency band, the pulses have a pulse width $T = 0.25$s, bandwidth $B = 2$kHz, and centre frequency $f_c = 2$kHz. It can be seen from Figs. 1*a* and *b* that the correlation of GSFM waveforms with different parameters is low. In addition, GSFM can also produce pulses that are nearly orthogonal to each other using the frequency reflection (FR) technique. Fig. 2 shows the IFs for four GSFM pulses with the same parameters α and ρ. Therefore, we can obtain a large number of nearly orthogonal GSFM waveforms within the same frequency band by combining the above two methods.

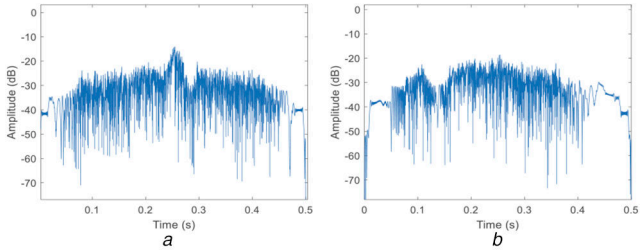

Fig. 1 *Cross-correlation of two GSFM pulses with different α and ρ*
(a) $\rho = 2.0$, $\alpha_1 = 160\,s^{-2}$, and $\alpha_2 = 192\,s^{-2}$, ***(b)*** $\rho_1 = 2.0$, $\rho_2 = 2.5$, and $\alpha = 160\,s^{-2}$

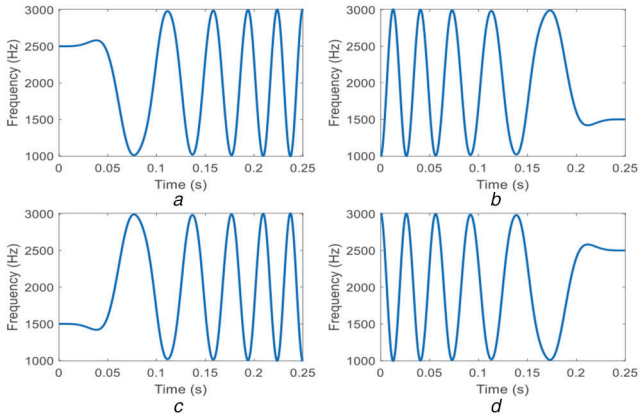

Fig. 2 *IF of the GSFM signal using FR with*
(a) Forward time, ***(b)*** Reverse time, ***(c)*** Forward time and flipped frequency, ***(d)*** Reverse time and flipped frequency

2.2 GSFM-com waveform

To maintain target detection performance while enabling the active sonar signal to carry data, we modulate the binary information into a GSFM waveform. Fig. 3 shows the combination of a digital BPSK signal and a GSFM waveform. This modulation can be done simply by multiplying the baseband binary pulse amplitude modulation (2PAM) signal (Fig. 3*b*) with the original GSFM signal (Fig. 3*a*). So, a GSFM-com signal can be expressed as:

$$\begin{aligned} y(t) &= a(t) \cdot g(t) \\ &= \sum_{i=0}^{N-1} b_i p(t - iT_b) \cdot g(t) \\ &= \sum_{i=0}^{N-1} b_i p(t - iT_b) \cdot \frac{\text{rect}(t)}{\sqrt{T}} e^{j\phi_{\text{GSFM}}(t)} e^{j2\pi f_c t}, \end{aligned} \tag{4}$$

where $a(t)$ is the baseband 2PAM signal containing N bits, b_i is the ith binary information bit, $p(t)$ is a rectangular pulse with unit height, and T_b is the duration of each symbol.

It can be seen from Fig. 3*c* that a GSFM-com signal obtained by multiplying a 2PAM and a GSFM signal is equivalent to introducing a 0 or π phase jump into the original GSFM signal for different data symbols:

$$y(t) = \sum_{i=0}^{N-1} p(t - iT_b) \cdot \frac{\text{rect}(t)}{\sqrt{T}} e^{j\phi_{\text{GSFM}}(t)} e^{j2\pi f_c t} e^{j\theta_i}, \quad (5)$$

where $\theta_i = 0$ if $b_i = 1$ and $\theta_i = \pi$ if $b_i = -1$.

Fig. 4*a* shows the spectrogram of a GSFM signal for parameters $\rho = 2.0$, $\alpha = 160\ \text{s}^{-2}$, pulse width 0.25 s, and bandwidth 2 kHz, where the starting frequency is 1 kHz and the ending frequency is 3 kHz. In Fig. 4*b*, compared with Fig. 4*a*, the bandwidth of the GSFM signal is expanded due to the embedded BPSK modulation.

Fig. 5 shows the autocorrelation of a GSFM signal and a GSFM-com signal. Both signals have pulse length $T = 0.25\,\text{s}$, centre frequency $f_c = 2\,\text{kHz}$, bandwidth $B = 2\,\text{kHz}$, and parameters $\rho = 2.0$ and $\alpha = 160\,\text{s}^{-2}$. The GSFM-com signal carries 250 bits of information. It can be seen from Fig. 5*a* that the highest sidelobe of the autocorrelation function of the GSFM signal reaches −9.1 dB, while the highest sidelobe of the autocorrelation function of the GSFM-com signal, as shown in Fig. 5*b*, is only −16.8 dB. So, the GSFM-com signal has better autocorrelation.

Fig. 6*a* shows the normalised peak of correlation processing for 20 GSFM-com pulses with ρ from 1 to 20 (step length is 1) when $\alpha = 160\,\text{s}^{-2}$. Fig. 6*b* shows the normalised peak of correlation processing for 21 GSFM-com pulses with α from 150 to 350 (step length is 10) when $\rho = 2.0$. All pulses have 250 bits of information and pulse length $T = 0.25$ s, centre frequency $f_c = 2\,\text{kHz}$, and bandwidth $B = 2\,\text{kHz}$. Thus, the GSFM-com signal still retains the near orthogonality of the GSFM signal when the bandwidth of the GSFM signal is much smaller than that of the BPSK signal. Fig. 7 is like Fig. 6 but the binary information in each GSFM-com pulse is different. It can be seen from Figs. 7*a* and *b* that the randomness of the binary information does not affect the near orthogonality of the GSFM-com signals.

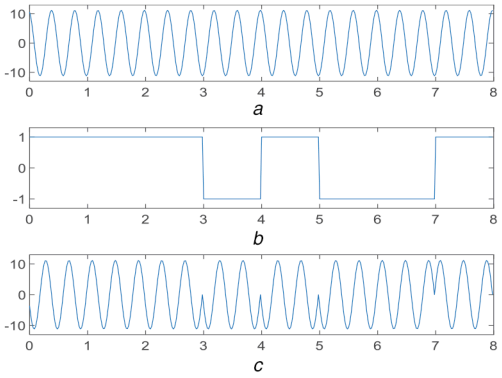

Fig. 3 *BPSK-modulated GSFM signal*
(a) Unmodulated GSFM signal, ***(b)*** Binary data, ***(c)*** GSFM-com signal

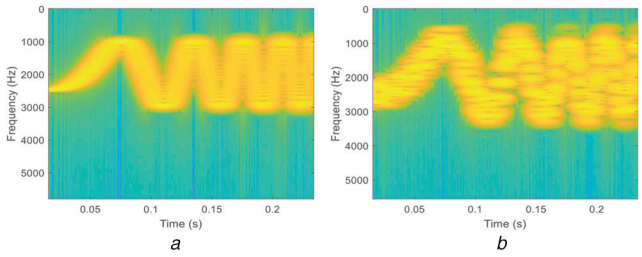

Fig. 4 *Spectrogram of*
(a) A GSFM signal, ***(b)*** A GSFM-com signal

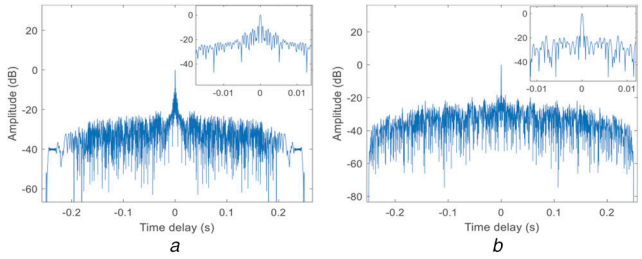

Fig. 5 *Autocorrelation for*
(a) A GSFM signal, ***(b)*** A GSFM-com signal

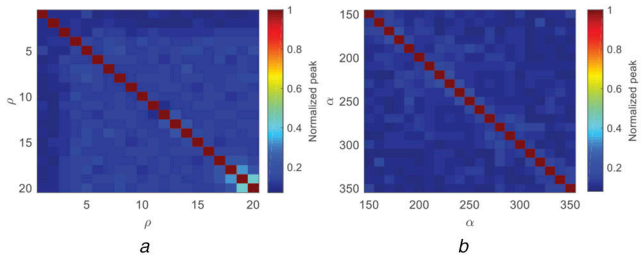

Fig. 6 *Orthogonal performance of GSFM-com signals with the same modulation information and different parameters*
(a) ρ from 1 to 20 (step length is 1) when $\alpha = 160\,\text{s}^{-2}$, ***(b)*** α from 150 to 350 (step length is 10) when $\rho = 2.0$

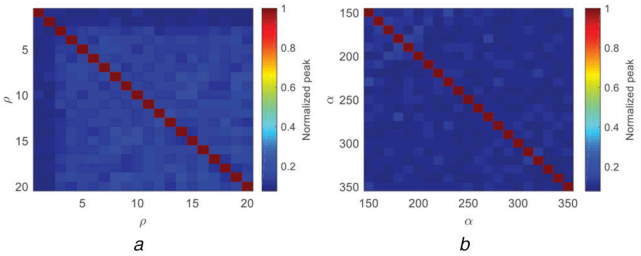

Fig. 7 *Orthogonal performance of GSFM-com signals with different modulation information and different parameters*
(a) ρ from 1 to 20 (step length is 1) when $\alpha = 160\,\mathrm{s}^{-2}$, ***(b)*** α from 150 to 350 (step length is 10) when $\rho = 2.0$

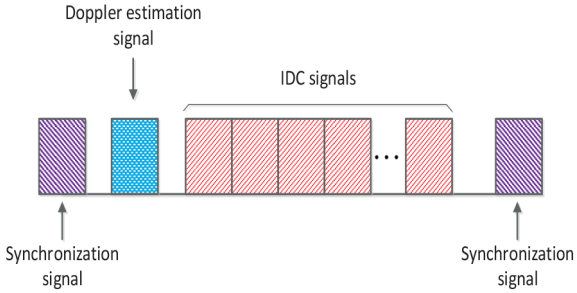

Fig. 8 *Frame format of the transmitted signal*

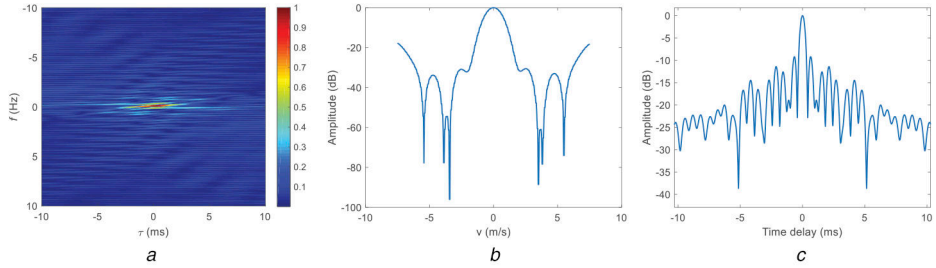

Fig. 9 *Auto-ambiguity function characteristics of GSFM signal*
(a) Auto-ambiguity function pseudo colour plot, ***(b)*** Zero-time-delay cut, ***(c)*** Zero-velocity cut

2.3 Transmit signal model

In this paper, we assume that the CAS-IDC system is constantly transmitting signals to search for targets and to communicate with friendly nodes. Fig. 8 shows the frame structure for the transmitted signal. An LFM signal is used for carrier and symbol synchronisation at the communication receiver. A Doppler estimation signal can use a continuous wave signal and a hyperbolic frequency-modulated signal. The latter is a Doppler tolerance signal that can estimate the Doppler shift from the offset of the correlation peak between the transmitter and the receiver. An IDC signal is a collection of GSFM-com signals that are nearly orthogonal to each other and transmitted sequentially. It is expressed as:

$$CS(t) = \frac{1}{\sqrt{NT_{\mathrm{PRI}}}} \sum_{n=1}^{N} y_n(t - (n-1)T_{\mathrm{PRI}}), \tag{6}$$

where N is the number of pulses in the integrated signal. The pulse repetition interval is equal to the individual GSFM-com pulse length: $T_{\mathrm{PRI}} = T$. Here, $y_n(t)$ is the nth GSFM-com pulse.

3 Detection performance of a GSFM-com signal

3.1 AF performance

A matched filter (MF) is an optimal receiver for signal detection in the presence of additive white Gaussian noise for both pulsed active sonar and CAS systems. When the target is stationary relative to the transmitter and receiver, the echo signal with a time delay τ will exactly match the MF. However, if the target is moving relative to the sonar system, the Doppler effect will occur, so that the received signal is extended or shrunk in the time domain. If the relative speed of the target and sonar system is v, the Doppler scaling factor is

$$\eta = \frac{1 + v/c}{1 - v/c}, \tag{7}$$

where c is the speed of acoustic waves in water.

The AF is the output of the MF calculated using the time delay τ and Doppler scaling factor η. The broadband AF measures the resolution of the pulse. The AF can be an auto-AF or a cross-AF. An auto-AF is generally used to measure the response of the MF for a pulse itself. The peak of the MF output is an estimate of the target distance and velocity. The auto-AF is defined as:

$$\chi_{n,n}(\tau, \eta) = \sqrt{\eta} \int g_n(t) g_n^*(\eta(t - \tau)) \mathrm{d}t\,. \tag{8}$$

The peak of the auto-AF occurs when $\tau = 0$ and $\eta = 1$. The cross-AF measures the cross-correlation between one pulse $g_m(t)$ and another pulse $g_n(t)$:

$$\chi_{m,n}(\tau, \eta) = \sqrt{\eta} \int g_m(t) g_n^*(\eta(t - \tau)) \mathrm{d}t\,. \tag{9}$$

In this paper, we are particularly interested in pulses that have a thumbtack auto-AF. They are sensitive to the Doppler shift like a continuous wave but also have a high range resolution like LFM. Figs. 9–11 show the time resolution and the frequency resolution of a GSFM signal, a BPSK signal and a GSFM-com signal, respectively. The parameters for GSFM in Figs. 9–11 are the same as for Fig. 6. Fig. 9*a* shows the auto-AF of the GSFM signal, Fig. 9*b* shows the zero-time-delay cut of the auto-AF, and Fig. 9*c*

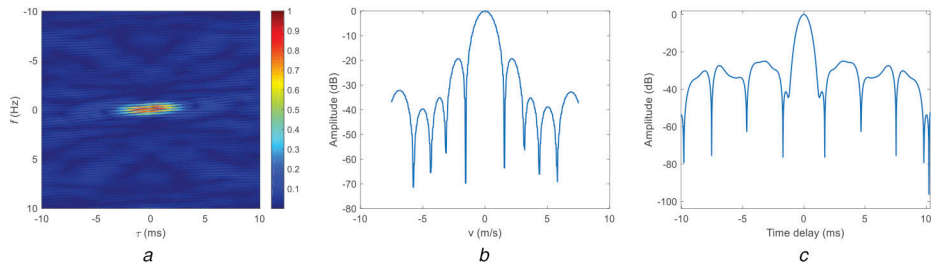

Fig. 10 *Auto-ambiguity function characteristics of BPSK signal*
(a) Auto-ambiguity function pseudo colour plot, ***(b)*** Zero-time-delay cut, ***(c)*** Zero-velocity cut

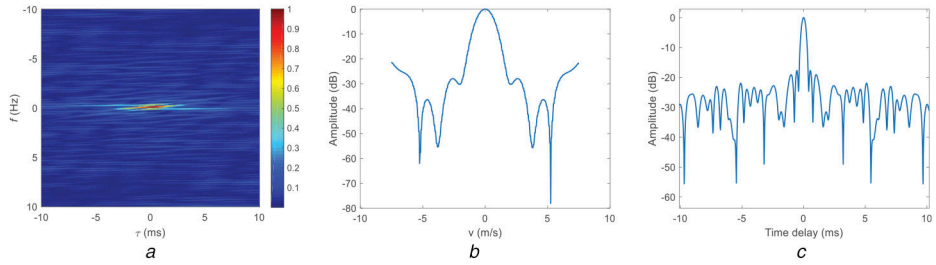

Fig. 11 *Auto-ambiguity function characteristics of GSFM-com signal*
(a) Auto-ambiguity function pseudo colour plot, ***(b)*** Zero-time-delay cut, ***(c)*** Zero-velocity cut

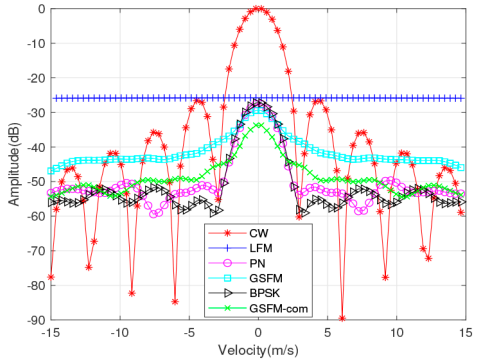

Fig. 12 *Q functions for different signal types*

shows the zero-velocity cut of the auto-AF. Fig. 10*a* shows the auto-AF of the BPSK signal, Fig. 10*b* shows the zero-time-delay cut of the auto-AF, and Fig. 10*c* shows the zero-velocity cut of the auto-AF. The BPSK signal has a pulse length $T = 0.25$ s, a centre frequency $f_c = 2$ kHz,and a bandwidth $B = 2$ kHz. The parameters for Fig. 11 are the same as those for Fig. 9. In addition, the BPSK signal has a bandwidth of 1 kHz. Fig. 11*a* shows the auto-AF of the GSFM-com signal, Fig. 11*b* shows the zero-time-delay cut of the auto-AF, and Fig. 11*c* shows the zero-velocity cut of the auto-AF. The auto-AFs for GSFM, BPSK and GSFM-com closely approximate a thumbtack AF according to Figs. 9*a*, 10*a* and 11*a*, but the GSFM-com auto-AF has a lower sidelobe. It can be seen from Figs. 9*b*, 9*c*, 11*b*, and 11*c* that the velocity resolutions of the GSFM signal and the GSFM-com signal are close, but the GSFM-com signal has a better range resolution than the GSFM signal. In addition, we can see from Figs. 10*c* and 11*c* that the mainlobe width of the GSFM-com signal's zero-velocity cut is narrower than that of the BPSK signal. Thus, the GSFM-com signal can more accurately separate two targets that are close in velocity and range.

3.2 Reverberation suppression

The Q function is called the waveform AF, it can be expressed as:

$$Q(\eta) = \int_{-\infty}^{\infty} \left| \chi(\tau, \eta) \right|^2 \mathrm{d}\tau \,. \tag{10}$$

The Q function is very significant for target detection with reverberation, and it is the integral of the square of the AF along the distance dimension. If we assume that the reverberation scatterer is stationary and that the reverberations are evenly distributed along the distance and have the same intensity, then the Q function represents the reverberation intensity of the MF output for different Doppler shifts. It can be used to measure the reverberation suppression for different waveforms. The smaller the Q function is, the smaller the reverberation output of the transmitted signal is, and the more beneficial it is for detecting a target. In contrast, the larger the Q function is, the more unfavourable it is for target detection.

Fig. 12 shows the Q function distribution for a GSFM signal, a BPSK signal, a GSFM-com signal, and three traditional active sonar signals, including a continuous wave signal, an LFM signal, and a pseudo-noise signal. In the simulation, for each signal, the pulse width $T = 0.25$ s, bandwidth $B = 2$ kHz, and centre frequency $f_c = 2$ kHz. In addition, the parameters for the GSFM and the GSFM-com signal are $\rho = 2.0$ and $\alpha = 160\,\mathrm{s}^{-2}$. The bandwidth of the GSFM signal in the GSFM-com signal is 500 Hz. As can be seen from Fig. 12, the reverberation suppression for the GSFM signal and the GSFM-com signal is significantly better than for the continuous wave and LFM signals commonly used in active sonar. Moreover, the reverberation suppression for the GSFM-com signal is better than for the GSFM signal. For low-speed targets, GSFM-com signals are the best for anti-reverberation of the six active sonar waveforms, while for high-speed targets, GSFM-com signals are only slightly worse than pseudo-noise signals and BPSK signals. Therefore, the proposed GSFM-com signal has excellent reverberation suppression performance.

4 Communication performance of GSFM-com signal

The delay spread of a UWA channel can easily reach tens or hundreds of milliseconds because of the low speed of acoustic waves (~1500 m/s) [24, 25]. In the frequency domain, the multipath effect leads to the selective fading of the frequency, which is equivalent to a comb filter. Therefore, after the transmitted signal passes through the UWA multipath channel, the signals for different frequency components will be attenuated to different degrees, resulting in large differences between the spectrum of the received signal and the spectrum of the transmitted signal. Unlike conventional single-carrier signals, GSFM-com signals transmit information using a broadband signal as the carrier. Due to the multipath effect, the waveform and spectrum of the signal are distorted. At the receiving end, we cannot completely remove the carrier in the GSFM-com signals, which leads to a degradation of performance. The bandwidth of the carrier signal is

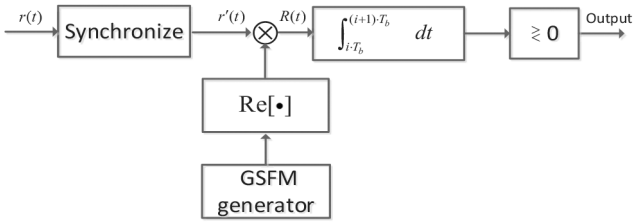

Fig. 13 *MFR for a GSFM-com signal*

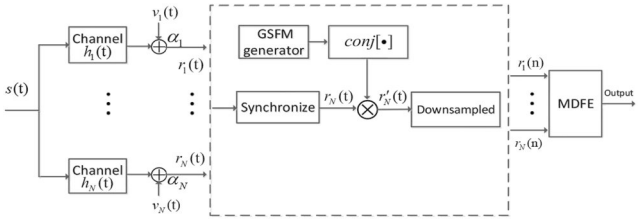

Fig. 14 *Multichannel DFER for a GSFM-com signal*

directly related to the stability of communications. In this section, we study the two receivers for a GSFM-com signal at the communication receiving end, namely MFR and DFER.

4.1 Matched filter receiver

Fig. 13 is a block diagram of the MFR for a GSFM-com signal at the communication receiving end. After synchronisation, Doppler estimation, and compensation, the received signal is multiplied by the real GSFM signal with the same parameters as the transmitted signal for demodulation:

$$\begin{aligned} R(t) &= r'(t) \cdot \mathrm{Re}[g(t)] \\ &= r'(t) \cdot \mathrm{Re}\left[\frac{\mathrm{rect}(t)}{\sqrt{T}} \mathrm{e}^{\mathrm{j}\phi_{\mathrm{GSFM}}(t)} \mathrm{e}^{\mathrm{j}2\pi f_c t}\right] \\ &= r'(t) \cdot \frac{\mathrm{rect}(t)}{\sqrt{T}} \cos(2\pi f_c t + \phi_{\mathrm{GSFM}}(t)), \end{aligned} \tag{11}$$

where $r'(t)$ is the received signal that has been synchronised and Doppler compensated, Re[a] denotes the real part of a. Next, a hard decision device is used to estimate the possible digital information in the GSFM-com signal.

4.2 Decision feedback equaliser receiver

First, the relationship between the communication performance of a GSFM-com signal and the bandwidth of the carrier GSFM signal is analysed theoretically. It is assumed that the transmitted signal is expressed as:

$$s(t) = a_n \cdot g(t), \tag{12}$$

where a_n is the transmitted baseband signal. The received signal passing through the UWA channel can be expressed as:

$$r(t) = s(t) \otimes h(t) + v(t), \tag{13}$$

where $\otimes$ is the convolution operation, $h(t)$ is the impulse response of the UWA multipath channel, and it is usually a time-varying function, especially for shallow water, $v(t)$ is the additive ambient noise in the passband. The demodulation at the receiving end occurs by multiplying by the local carrier:

$$\begin{aligned} r'(t) &= r(t) \cdot g'(t) \\ &= (a_n \cdot g(t)) \otimes h(t) \cdot g'(t) + v(t) \cdot g'(t) \\ &= (a_n \cdot g(t)) \otimes h(t) \cdot g'(t) + v'(t), \end{aligned} \tag{14}$$

where $g'(t)$ is the conjugate of $g(t)$ and $v'(t)$ represents the additive ambient noise in the baseband. The GSFM signal can be represented by several single-frequency signals:

$$g(t) = \sum_{i=1}^{N} A_i \mathrm{e}^{\mathrm{j}2pif_i} = \sum_{i=1}^{N} c_i, \tag{15}$$

where f_1 denotes the lower limit frequency of the GSFM signal, f_N denotes the upper limit frequency of the GSFM signal, and A is the amplitude coefficient. So (14), can be expressed as:

$$\begin{aligned} r'(t) &= \left(a_n \cdot \sum_{i=1}^{N} c_i\right) \otimes h(t) \cdot \sum_{i=1}^{N} c_i' + v'(t) \\ &= (a_n \cdot (c_1 + c_2 + \cdots + c_N)) \otimes h(t) \\ &\quad \cdot (c_1' + c_2' + \cdots + c_N') + v'(t) \\ &= (a_n \cdot c_1 \otimes h(t) + a_n \cdot c_2 \otimes h(t) + \cdots + a_n \cdot c_N \otimes h(t)) \\ &\quad \cdot (c_1' + c_2' + \cdots + c_N') + v'(t) \\ &= a_n \cdot c_1 \otimes h(t) \cdot c_1' + a_n \cdot c_1 \otimes h(t) \cdot c_2' + \cdots \\ &\quad + a_n \cdot c_1 \otimes h(t) \cdot c_N' + a_n \cdot c_2 \otimes h(t) \cdot c_1' \\ &\quad + a_n \cdot c_2 \otimes h(t) \cdot c_2' + \cdots + a_n \cdot c_2 \otimes h(t) \cdot c_N' \\ &\quad + a_n \cdot c_N \otimes h(t) \cdot c_1' + a_n \cdot c_N \otimes h(t) \cdot c_2' + \cdots \\ &\quad + a_n \cdot c_N \otimes h(t) \cdot c_N' + v'(t), \end{aligned} \tag{16}$$

where c_i' is the conjugate of c_i. Here, $a_n \cdot c_i \otimes h(t) \cdot c_j'$ $(i = j)$ has the same demodulation form as a single-carrier system. Then, $r'(t)$ is processed with low-pass filtering, and the frequency response of the filter is

$$E(f) = \begin{cases} 1, & f < f_b, \\ 0, & \text{other}, \end{cases} \tag{17}$$

where f_b denotes the upper limit frequency of the baseband signal a_n. The output of the low-pass filter can be expressed as:

$$\begin{aligned} r''(t) &= \int_{-\infty}^{\infty} r'(t) \cdot e(t-\tau)\mathrm{d}\tau \\ &= N \cdot a_n \otimes h(t) + \sum_i \sum_j a_n \cdot c_i \otimes h(t) \cdot c_j' + v''(t) \\ &= l(t) + m_{i,j}(t) + v''(t), \end{aligned} \tag{18}$$

where $i \not= j$, $i > j$, and $f_i - f_j \le f_b$. Here

$$l(t) = N \cdot a_n \otimes h(t) \tag{19}$$

and

$$m_{i,j}(t) = \sum_i \sum_j a_n \cdot c_i \otimes h(t) \cdot c_j', \tag{20}$$

where $i \neq j$, $i > j$, and $f_i - f_j \le f_b$.

Here $l(t)$ has removed the carrier signal completely. $v''(t)$ is the demodulated and filtered noise interference and $m_{i,j}(t)$ is the interference term that carries part of the carrier after demodulating and filtering. It is obvious that $m_{i,j}(t)$ is related to the upper limit frequency of the baseband signal f_b and the bandwidth of the carrier signal. The higher the upper limit frequency of the baseband signal is, the stronger the interference after demodulation. The larger the bandwidth of the carrier GSFM signal is, the stronger the interference after demodulation. Therefore, a carrier GSFM signal should use a bandwidth appropriate for the actual UWA channel.

Fig. 14 is a block diagram of a multichannel DFER for a GSFM-com signal at the communication receiving end. First, signals received from each channel are synchronised, Doppler estimated, and compensated, and then they are demodulated by multiplying the conjugate of the GSFM signal with the same parameters used for the transmitted signal. The demodulation of the signal received from the channel N can be expressed as:

$$r'_N(t) = r_N(t) \cdot \mathrm{conj}[g(t)]$$
$$= r_N(t) \cdot \frac{\mathrm{rect}(t)}{\sqrt{T}} \cdot \mathrm{conj}\left[e^{j\phi_{\mathrm{GSFM}}(t)} e^{j2\pi f_c t}\right], \quad (21)$$

where $r_N(t)$ is the signal of the channel N that has been synchronised, conj[a] denotes the conjugate of a. After the signal of each channel is downsampled, we can use the multichannel DFER to decode it. A decision feedback equaliser can suppress the inter-code interference in the received signal to a certain extent through adaptive equalisation, which improves the performance of the receiver system.

4.3 Comparison of MFR and single-channel DFER

Fig. 15*a* shows the sound velocity profile measured in the experiment in Songhua Lake, Jilin Province, in July 2019. There is an obvious negative sound velocity gradient. Fig. 15*b* shows the multipath channel between the transmitter and receiver calculated using Bellhop. In the simulation, the depths of the transmitter and receiver are 10 and 15 m, respectively, and the horizontal distance between them is 800 m. The parameters were as follows: sampling rate $f_s = 48$ kHz, centre frequency $f_c = 2$ kHz, $\rho = 2.0$, and $\alpha = 160\,\mathrm{s}^{-2}$. The pulse width of the GSFM-com signal was $T = 10$ s, and the symbol rate was 1000 symbols/s. The training sequence length for DFER was set to 500.

First, the performance of MFR was studied. The bandwidth of the GSFM signal in the simulation was 500 Hz. Fig. 16 shows the bit error rate (BER) decoded by MFR with or without multipath interference. It can be seen that the decoding performance of MFR increases with an increase of the signal-to-noise ratio (SNR) when there is no multipath interference, but it is very sensitive to multipath interference and is not suitable for the UWA environment with strong multipath interference.

Next, we set the bandwidth of the GSFM signal in GSFM-com as 100, 200, 500, 1000, and 1500 Hz in turn, and simulated the performance of DFER. The multipath channel shown in Fig. 15*b* was still used. The number of taps of the forward filter and feedback filter was 20, and the ratio of the phase-locked loop and sparse scores were 0.0001 and 0.00001, respectively. Fig. 17 shows the BER decoded by DFER with different bandwidths for GSFM signals and SNR. The bandwidth of the GSFM signals was 500, 1000, and 1500 Hz. When the SNR was higher than 4 dB, the BER of DFER can be as low as 10^{-4}. The decoding performance of DFER was significantly improved when the bandwidth of GSFM signals was 100 or 200 Hz. In actual use, the length of the training sequence and the number of filter taps should be adjusted according to the channel multipath delay to ensure stable and balanced performance.

5 Experimental results

An UWA communication experiment was carried out in Songhua Lake, China, in December 2019. GSFM-com signals with a GSFM signal bandwidth of 100, 200, and 500 Hz were transmitted. Other system parameters were as shown in Table 1. The LFM signal is the synchronisation signal. Fig. 18 shows the layout of the experiment. T represents the transmitting transducer. It had a frequency band of 8–20 kHz and was deployed from a surface vessel to a depth of 10 m. A 32-element hydrophone array was vertically distributed with an interval of 1 m. The top hydrophone was 2 m from the water surface. Each element is represented by H_n

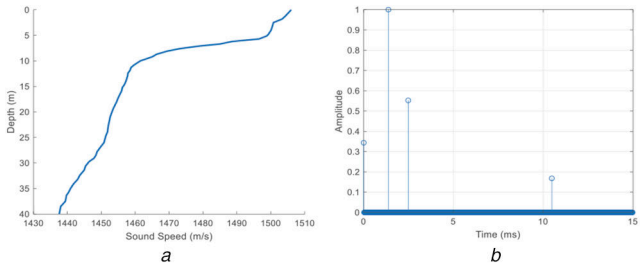

Fig. 15 *The simulation environment*
(a) Measured sound speed profile, ***(b)*** Multipath UWA channel

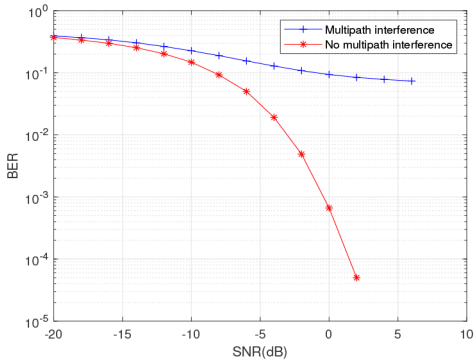

Fig. 16 *BER performance of MFR*

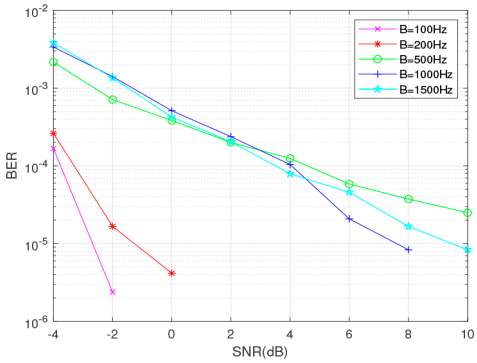

Fig. 17 *BER performance of DFER. (B is the bandwidth of the GSFM signal.)*

Table 1 Parameters of the transmitted signal

Description	Value
sampling rate	96 kHz
pulse width of GSFM-com	10 s
transmitted data	5000 bits
training sequence	500 bits
mapping	BPSK
roll-off factor	1
symbol rate	500 symbols/s
pulse width of LFM	0.5 s
frequency band of LFM	8–20 kHz
guard interval	0.2 s
ρ	2.0
α	160 s^{-2}

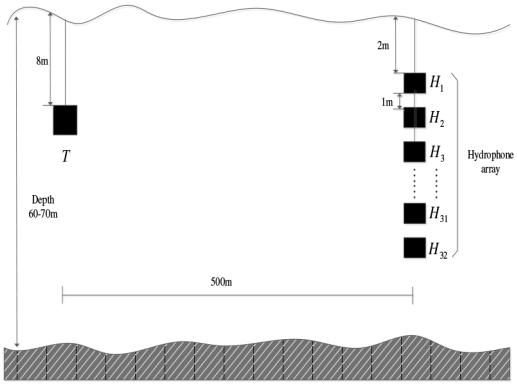

Fig. 18 *Experimental layout*

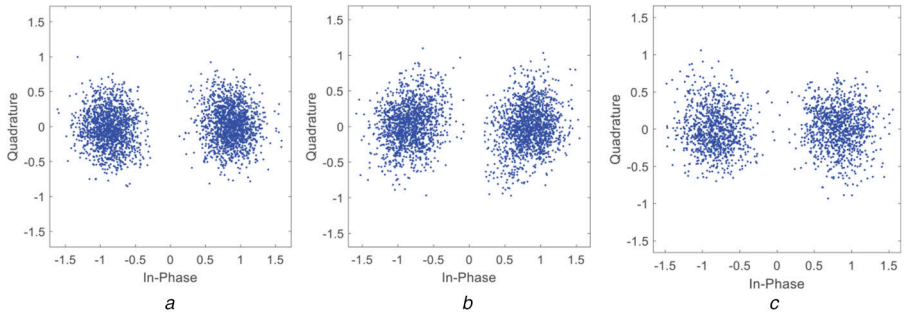

Fig. 19 *Results for single-channel DFER when the bandwidth of the GSFM signal was* ***(a)*** 100 Hz, ***(b)*** 200 Hz, ***(c)*** 500 Hz

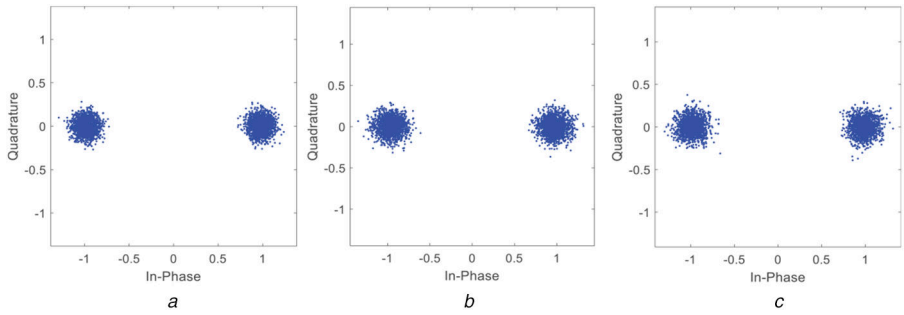

Fig. 20 *Results for 8-channel DFER when the bandwidth of the GSFM signal was* ***(a)*** 100 Hz, ***(b)*** 200 Hz, ***(c)*** 500 Hz

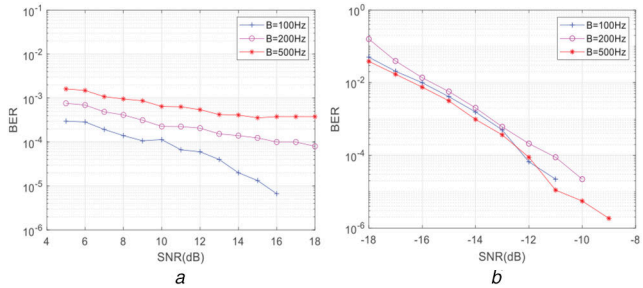

Fig. 21 *BER for different SNRs for* ***(a)*** Single-channel DFER, ***(b)*** 8-channel DFER. (B is the bandwidth of the GSFM signal.)

($n = 1, 2, \ldots, 32$). The horizontal distance of the array from the acoustic source was ∼500 m.

In this paper, single-channel DEFR and 8-channel DEFR are applied to process the data collected by hydrophones. The number of taps of the forward filter and feedback filter were 15 and 30, respectively. The ratio of the phase-locked loop and sparse scores were 0.0001 and 0.00001, respectively. Fig. 19 shows the results for single-channel DEFR for the three GSFM-com signals. Figs. 19*a–c* are scatterplots of the equalised symbols of the signals received by H_8. The output SNRs after the equalisation were 8.6328, 7.6012, and 7.7215 dB. Fig. 20 shows the results for 8-channel DEFR for the three GSFM-com signals. Figs. 20*a–c* are scatterplots of the equalised symbols for eight joint elements: H_3, H_4, H_5, H_6, H_7, H_8, H_9, and H_{10}. The output SNRs after equalisation were 18.8288, 17.0153, and 16.7459 dB. So we can conclude that high gains can be achieved when using hydrophones array.

According to the calculation, the SNR of the signal received from each element was about 28.6 dB. We artificially added noise to the signal received from each element to reduce the SNR to study the performance of DFER under different SNRs. The results are shown in Fig. 21. The performance of 8-channel DFER is much better than that of single-channel DFER, which can almost achieve zero BER communications when SNR > −10 dB.

In this paper, the received signals are regarded as target echo signals. Fig. 22 shows the cross-AF of the first 0.5 s of the received signal and local GSFM-com signal. The bandwidth of the GSFM signal was 200 Hz. In Fig. 22*b*, the horizontal axis represents the time delay and the vertical axis represents the target speed. The time delay from the transmitter to the receiver was 333 ms and the speed of the transmitter was 0 m/s.

6 Conclusion

A novel IW for CAS detection and communication was presented in this paper. A GSFM-com signal can be obtained by embedding BPSK modulation into a GSFM signal. In terms of detection, the

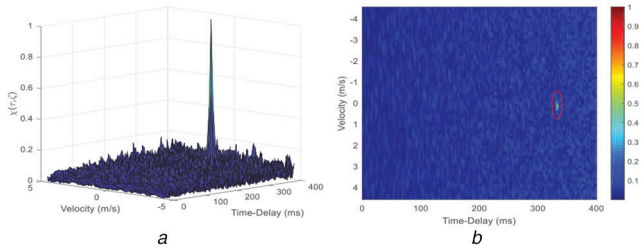

a *b*

Fig. 22 *Cross-ambiguity function of the first 0.5 s of the received signal and the local GSFM-com signal*
(a) Contour plot, ***(b)*** Pseudo colour plot

modulation of random information still retains the near orthogonality of the GSFM signal, so that a GSFM-com signal can be applied in a CAS system. In addition, the analysis of the AF and Q function showed that a GSFM-com signal has better time-frequency resolution and reverberation suppression than a GSFM signal. In terms of communication, the multipath effect severely limits the performance of MFR, which cannot be applied in a multipath serious shallow water environment. The experimental results show that multichannel DFER can eliminate the inter-code interference caused by the multipath effect and maintain stable decoding performance at a lower SNR. Future work will focus on optimising the GSFM-com signal and on-field experiments of CAS-IDC.

7 Acknowledgments

This research was funded by the National Natural Science Foundation of China (61631008, 61901136, 51779061), the National Key R&D Program of China (2018YFC1405900), the Fok Ying-Tong Education Foundation (151007), and the Innovation Special Zone of National Defense Science and Technology.

8 References

[1] Mealey, R.M.: 'A method for calculating error probabilities in a radar communication system', *IEEE Trans. Space Electron. Telemetry*, 1963, **9**, (2), pp. 37–42
[2] Coleman, J.O.: 'Architecture for a demonstration radar-communication link', Naval Research Lab Report, 1984
[3] Lu, J., Zhang, Q.F., Zhang, L.L., *et al.*: 'Detection performance of active sonar based on underwater acoustic communication signals'. IEEE Int. Conf. on Signal Processing, Communications and Computing, Qingdao, China, 2018
[4] Jankiraman, M., Wessels, B.J., Genderen, E.: 'Pandora multifrequency FMCW/SFCW radar'. IEEE Int. Radar Conf., Alexandria, VA, USA, 2000
[5] Jankiraman, M., De Jong, E.W., Van Genderen, P.: 'Ambiguity analysis of PANDORA multifrequency FMCW/SFCW radar'. IEEE Int. Radar Conf., Alexandria, VA, USA, 2000
[6] Levanon, N.: 'Multifrequency complementary phase-coded radar signal', *IEEE Proc. Radar, Sonar Navig.*, 2000, **147**, (6), pp. 276–284
[7] Levanon, N., Mozeson, E.: '*Radar signals*' (Wiley Interscience, Hoboken, NJ, 2004), ch. 11
[8] Xu, S.J., Chen, Y., Zhang, P.: 'Integrated radar and communication based on DS-UWB'. 3rd Int. Conf. on Ultrawideband and Ultrashort Impulse Signals, Sevastopol, Ukraine, 2006, pp. 142–144
[9] Jamil, M., Zepernick, H.J., Pettersson, M.I.: 'On integrated radar and communication systems using oppermann sequences'. IEEE Military Communications Conf., San Diego, CA, USA, 2009
[10] Xie, Y., Tao, R., Wang, T.: 'Method of waveform design for radar and communication integrated system based on CSS'. 1st Int. Conf. on Instrumentation. IEEE Computer Society, Beijing, China, 2011
[11] Chen, X., Wang, X., Xu, S., *et al.*: 'A novel radar waveform compatible with communication'. Int. Conf. on Computational Problem-solving, Chengdu, China, 2011
[12] Roberton, M., Brown, E.: 'Integrated radar and communications based on chirped spread-spectrum techniques'. Int. Microwave Symp. Digest, Philadelphia, PA, USA, 2003
[13] Zhang, Z., Nowak, M.J., Yang, Q., *et al.*: 'RF steganography via LFM chirp radar signals', *IEEE Trans. Aerosp. Electron. Syst.*, 2017, **PP**, (99), pp. 1–1
[14] Nowak, M., Wicks, M., Zhang, Z., *et al.*: 'Co-designed radar-communication using linear frequency modulation waveform', *IEEE Aerosp. Electron. Syst. Mag.*, 2016, **31**, (10), pp. 28–35
[15] Zhang, Z., Nowak, M.J., Wicks, M., *et al.*: 'Bio-inspired RF steganography via linear chirp radar signals', *IEEE Commun. Mag.*, 2016, **54**, (6), pp. 82–86
[16] Murphy, S.M., Scrutton, J.G.E., Hines, P.C.: 'Experimental implementation of an echo repeater for continuous active sonar', *IEEE J. Ocean. Eng.*, 2016, **PP**, (99), pp. 1–9
[17] Liang, J., Xu, L., Li, J., *et al.*: 'On designing the transmission and reception of multistatic continuous active sonar systems', *IEEE Trans. Aerosp. Electron. Syst.*, 2014, **50**, (1), pp. 285–299
[18] Lepage, K.D., Canepa, G., Bates, J., *et al.*: 'Bistatic continuous active sonar processing using arrays towed from unmanned underwater vehicles', *J. Acoust. Soc. Am.*, 2017, **141**, (5), p. 3850
[19] Hines, P.C., Murphy, S.M., Hicks, K.T.: 'Comparison of signal coherence for continuous active and pulsed active sonar measurements in littoral waters', *J. Acoust. Soc. Am.*, 2014, **136**, (4), p. 2226
[20] Hague, D.A., Buck, J.R.: 'A generalized sinusoidal frequency modulated waveform for continuous active sonar'. Conf. IEEE Oceans – Genova, Genoa, Italy, September 2015
[21] Hague, D.A., Buck, J.R.: 'A generalized sinusoidal frequency-modulated waveform for active sonar', *IEEE J. Ocean. Eng.*, 2017, **42**, (1), pp. 109–123
[22] Zhang, G.S., Dong, H.F.: 'Spatial diversity in multichannel processing for underwater acoustic communications', *Ocean Eng.*, 2011, **38**, (14), pp. 1611–1623
[23] Han, X., Yin, J.W., Tian, Y.N., *et al.*: 'Underwater acoustic communication to an unmanned underwater vehicle with a compact vector sensor array', *Ocean Eng.*, 2019, **184**, pp. 85–90
[24] van Walree, P., Jenserud, T., Smedsrud, M.: 'A discrete-time channel simulator driven by measured scattering functions', *IEEE J. Sel. Areas Commun.*, 2008, **26**, pp. 1628–1637
[25] Stojanovic, M., Preisig, J.: 'Underwater acoustic communication channels: propagation models and statistical characterization', *IEEE Commun. Mag.*, 2009, **47**, pp. 84–89